Hindawi Publishing Corporation
Advances in Meteorology
Volume 2016, Article ID 2089418, 15 pages
http://dx.doi.org/10.1155/2016/2089418

Research Article

Impacts of Wind Stress Changes on the Global Heat Transport, Baroclinic Instability, and the Thermohaline Circulation

Jeferson Prietsch Machado,[1] Flavio Justino,[2] and Luciano Ponzi Pezzi[3]

[1]*Universidade Estadual Paulista Júlio de Mesquita Filho (UNESP), 17012-633 Bauru, SP, Brazil*
[2]*Universidade Federal de Viçosa (UFV), 36570-000 Viçosa, MG, Brazil*
[3]*Instituto Nacional de Pesquisas Espaciais (INPE), 12227-010 São José dos Campos, SP, Brazil*

Correspondence should be addressed to Jeferson Prietsch Machado; jefpmac@gmail.com

Received 9 August 2015; Revised 5 November 2015; Accepted 29 November 2015

Academic Editor: Leonard J. Pietrafesa

The wind stress is a measure of momentum transfer due to the relative motion between the atmosphere and the ocean. This study aims to investigate the anomalous pattern of atmospheric and oceanic circulations due to 50% increase in the wind stress over the equatorial region and the Southern Ocean. In this paper we use a coupled climate model of intermediate complexity (SPEEDO). The results show that the intensification of equatorial wind stress causes a decrease in sea surface temperature in the tropical region due to increased upwelling and evaporative cooling. On the other hand, the intensification of wind stress over the Southern Ocean induces a regional increase in the air and sea surface temperatures which in turn leads to a reduction in Antarctic sea ice thickness. This occurs in association with changes in the global thermohaline circulation strengthening the rate of Antarctic Bottom Water formation and a weakening of the North Atlantic Deep Water. Moreover, changes in the Southern Hemisphere thermal gradient lead to modified atmospheric and oceanic heat transports reducing the storm tracks and baroclinic activity.

1. Introduction

The coupling between the atmosphere and ocean has been investigated by several studies. The pioneer works by Walker and Bilss [1], Bjerknes [2], and Wyrtki [3] are the starting point to the understanding of the El Niño-Southern Oscillation (ENSO), the air-sea interaction, and the decadal climate variability. Recently, studies have analyzed the impacts caused by fluctuations of wind stress on oceanic and atmospheric circulations [4–10]. This recent motivation is directly related to climate projections for the coming decades. In this context, numerical models designed with the increase in the concentration of CO_2 in the atmosphere indicate a maximum displacement of wind stress to higher latitudes than normal, due to the intensification of the winds in extratropical latitudes [11–14]. On this hypothesis, it becomes important to numerical climate simulations forced by wind stress anomalies to analyze the impacts caused on the oceanic and atmospheric circulations. In the following several studies based on numerical modeling will be shown, demonstrating the importance of wind stress for the coupling between the atmosphere and ocean.

McCreary and Lu [15] and Liu and Philander [16] argued that the strength of the oceanic subtropical cells as well as the magnitude of the equatorial upwelling is tightly dependent on the wind stress near 10°N–20°N. One should expect that changes in the magnitude of the winds can intensify the vertical oceanic circulation through changes in the Ekman transport. Indeed, an intensification of the equatorial wind stress by about 30–50% leads to an enhancement of the meridional water transport by about 2 Sv (1 Sverdrup = 10^6 m^3 s^{-1}) and an equatorial cooling of approximately 2°C. This has been a common feature in climate simulations focusing on the Last Glacial Maximum [17–19]. It is noteworthy that England et al. [20] showed that a pronounced strengthening in Pacific trade winds over the past two decades is sufficient to account for the cooling of the tropical Pacific and a substantial slowdown in surface warming through increased subsurface ocean heat

uptake. Furthermore, they showed that the accelerated trade winds have increased equatorial upwelling in the central and eastern Pacific, lowering sea surface temperature (SST) there, which drives further cooling in other regions.

On the other hand, Timmermann and Goosse [6] and MacMynowski and Tziperman [21] highlighted the importance of the wind stress to the global thermohaline circulation (THC). The wind stress changes on the Southern Ocean may also be responsible for modulating the intensity of the Atlantic Meridional Overturning Circulation (MOC) [22]. These wind-induced changes of the MOC can regulate the glacial-interglacial periods due to changes in air-sea CO_2 fluxes [23–25]. Timmermann and Goosse [6], by disregarding the influence of wind stress, have found an interruption in the MOC. This has been attributed to changes in the equator-pole density gradient which is not maintained without the wind stress forcing, because the wind stress contributes to the horizontal transport of salinity due to the wind-driven circulation. It plays also an important role in the vertical transport of salinity and in the oceanic convection due to Ekman pumping.

Also it is important to highlight how the wind stress influences the oceanic and atmospheric circulation patterns at mid and high latitudes of the Southern Hemisphere. In the study made by Yang et al. [7] they analyze changes in wind stress for decadal periods in the Southern Ocean and associated with ozone depletion in the Antarctic region. These authors used the 40 years of European Centre for Medium-Range Weather Forecasts (ECMWF) Reanalysis (ERA 40) data and found an increasing wind stress trend between latitudes of 45°S and 60°S in the past 20 years. According to the authors, this occurs due to the wind anomalies due to the Antarctic Oscillation, which interacts with the medium flow and meridional circulation.

Menviel et al. [8], based on LOVECLIM climate simulations, found that 15% intensification of the near surface winds between 40°S and 60°S increases the Antarctic Bottom Water (AABW) rate of formation from 16 to 32 Sv.

Saenko [9] examining the impact of the wind stress changes on SSTs has demonstrated surface temperature reduction at high latitudes accompanied by increased sea ice area. Changes in the wind stress are also responsible for increasing the atmospheric poleward heat transport in both hemispheres due to modulation of the storm tracks [26].

Ma et al. [10] concluded that an absence of wind stress over 40°S leads to a reduction of approximately 50% in the MOC. This reveals the strong coupling between the atmosphere and the ocean at high latitudes as well as its control on the THC. Indeed, the absence of wind stress in 40°S leads to a reduction of vertical mixing and upwelling, inducing the surface cooling and sea ice expansion. However, warming is observed in subsurface waters due to the weakening of the vertical mixing.

Recently, Machado et al. [27] showed that the wind stress intensification in the equatorial region causes changes in Atlantic Dipole and enhanced precipitation over Brazilian northeast. Moreover, the wind stress intensification in the extratropical Southern Hemisphere region induces weakening of positive Antarctic Oscillation phase.

Therefore, the aim of this study is to analyze the oceanic and atmospheric circulation response to increased wind stress at different latitudes in the SH. We also focus on the baroclinic instability and storm tracks changes as well as on the identification of the main changes in the atmospheric and oceanic heat transport. In particular, changes in the global thermohaline circulation are analyzed. It should be stressed that the response of the atmospheric and oceanic heat transport to modified wind stress has been partially overlooked in the literature.

This paper is organized as follows: Section 2 provides a description of the numerical coupled model used and details on the employed methodology. Section 3 shows the anomalies found in atmospheric and oceanic circulations. This study presents in Section 4 the conclusions and final remarks.

2. Numerical Model and Experiments Design

This study is based on simulations conducted with the coupled climate model Speedy-Ocean (SPEEDO) [28]. SPEEDO may be classified as an Earth system model of intermediate complexity. This model was chosen in order to fill a gap between the global models, which have physical representation quite complex and conceptual models, which are rather simplified [28].

The atmospheric component of the SPEEDO coupled model, called Simplified Parameterization primitivE-Equation Dynamics (SPEEDY), is a hydrostatic spectral model with 8 vertical layers (925, 850, 700, 500, 300, 200, 100, and 30 hPa) and horizontal truncation T30, which corresponds to a horizontal resolution of 3.75°. This uses the divergence-vorticity equation as described by Bourke [29]. The parameterizations include the short- and long-wave radiation schemes, large-scale condensation and convection, momentum, heat and humidity fluxes, and vertical diffusion processes. The convection is represented by a mass flow scheme that is activated when conditional instability occurs. This version is coupled to physical parameterizations for the hydrological cycle [30]. Additional details about the model formulation can be found in Molteni [31].

Although the atmospheric model proposed in the study is of intermediate resolution, previous studies showed its ability to reproduce the main features of the climate system both in tropical latitudes and extratropical regions [28, 31–34]. A detailed comparison between the simulated climate by SPEEDY and CCM3 and ERA40 models can be seen at http://esp.ictp.it.

The oceanic component of the SPEEDO is the *Coupled Large-Scale Ice-Ocean model* (CLIO) [35]. This model is based on the primitive equations (Navier-Stokes equations) and uses free surface with thermodynamic/dynamic parameterization for the sea ice component. CLIO also employs parameterizations for vertical diffusivity, which is a simplification of the Mellor and Yamada turbulence scheme [36]. The oceanic model includes parameterizations of vertical and horizontal mixing and turbulent diffusion processes along the isopycnals to represent the effect of mesoscale turbulent eddies in the ocean transport [37].

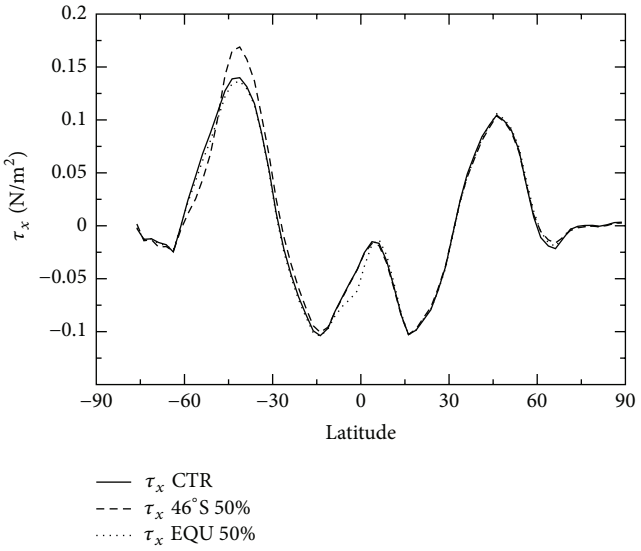

Figure 1: Annual wind stress zonally averaged τ_x (N/m^2) for the CTR, EQU 50%, and 46°S 50% simulations.

The CLIO horizontal resolution is approximately 3° of latitude and longitude, with 20 vertical levels unevenly spaced. The model has more levels concentrated close to the surface in order to better represent the oceanic processes that occur in the oceanic mixing layer.

The investigation made here is based on three climate sensitivity experiments: the control simulation (CTR), which was run for 200 years taking into account the current conditions of albedo, vegetation, and topography. The same boundary conditions were employed to another two simulations, however, intensifying the wind stress by 50%. The modified wind stress was applied over two regions, centered at the 1°S of latitude (EQU 50%) and 46°S of latitude (46°S 50%).

In order to investigate the influence of the wind stress to changes on the climate, the forcing function in the meridional direction is multiplied with the simulated zonal wind stress component. The function is defined as

$$\left[1 + a * e\left[\frac{2(\gamma r - \gamma)^2}{\alpha}\right]\right], \quad (1)$$

where "a" is the amplitude factor, "γr" is the latitude anomaly maximum, and "α" is the width of the anomalous wind stress forcing. The EQU 50% experiment is based on an increase by 50% of wind stress in the equatorial region; that is, the factor "a" was regarded as 0.5 and "γr" the value of 1°S latitude on CLIO model. The third simulation (46°S 50%) also considered the amplitude factor of 0.5, but with the wind stress changes applied to the latitude of 46°S. The reasoning behind the use of this function is to prevent border problems in simulations; that is, it acts as a damping factor, which has a maximum value at the latitude chosen, which will decrease as initial latitude.

Figure 1 shows a zonal average τ_x for the three simulations, which is taken from the average of τ_x values for all longitude points, while the values vary for each latitude, taking the average of the past twenty years for each experiment (1980–1999). Note that by multiplying τ_x by β function, there is an increase in the wind stress, with major differences in 1°S (dotted line) and 46°S (dashed line), falling within a range of approximately 15° to the two simulations.

3. Results and Discussion

3.1. Oceanic Changes

3.1.1. Sea Surface Temperature and Antarctic Sea Ice. The annual mean climate simulated by SPEEDO has been discussed extensively by Severijns and Hazeleger [28] and Justino et al. [34]; thus no effort will be done to describe this in detail. The 50% increase in the wind stress in the equatorial region and 46°S generates distinct climate responses. Indeed, wind stress increasing in the equatorial region induces a cooling of the equatorial Pacific by up to 2°C (EQU 50%, Figure 2(a)). Decreasing of SST is also noted in the tropical Atlantic and Indian Oceans, with values of about 1°C. Similar results were obtained by Klinger et al. [38] and Liu and Philander [16], due to stronger upwelling in the region and associated strengthening of the oceanic vertical cells. Therefore, the intensification of wind stress in the equatorial region causes a pattern similar to the La Niña condition, being associated with the Ekman transport. The oceanic Ekman transport and pumping are among the most important parameters in studying the ocean general circulation and its variability. Upwelling due to the Ekman transport divergence has been identified as a leading mechanism for the seasonal to interannual variability of the upper-ocean heat content in many parts of the World Ocean, especially along coasts and the equator [39].

On the other hand, positive SST anomalies are found in the SH extratropical region by changing the wind stress at 46°S (46°S 50% experiment, Figure 2(b)) with values of up to 3°C; small values are found throughout the Global Ocean. Differently the Nordic Sea experiences a drop in SST values. The observed anomalies SST in 46°S 50% show a reverse pattern to that in EQU 50%; that is, they may be associated with a condition of Ekman pumping. The Ekman pumping is the primary mechanism that drives basin-scale circulations in subtropical and subpolar oceans [39]. Therefore, alterations in the transport Ekman in extratropical latitudes favor the changes in water masses and, consequently, they can cause changes on the THC associated with the weakening of the North Atlantic Deep Water (NADW). The changes in THC will be shown later.

However, changes in the wind stress in extratropical regions are not yet clear. According to Ma et al. [10], weaker wind stress over high latitudes of the SH leads to negative SST anomalies of 2°C in the Pacific between 40°S and 60°S, while a warming of up to 0.5°C is observed in the Atlantic. Delworth and Zeng [40] argued that SST anomalies due to an intensification of the wind stress in the Southern Ocean do not occur uniformly. They found positive anomalies of about 2°C between the Atlantic and the Indian Ocean, related to the displacement of warm water of subtropical origin. However,

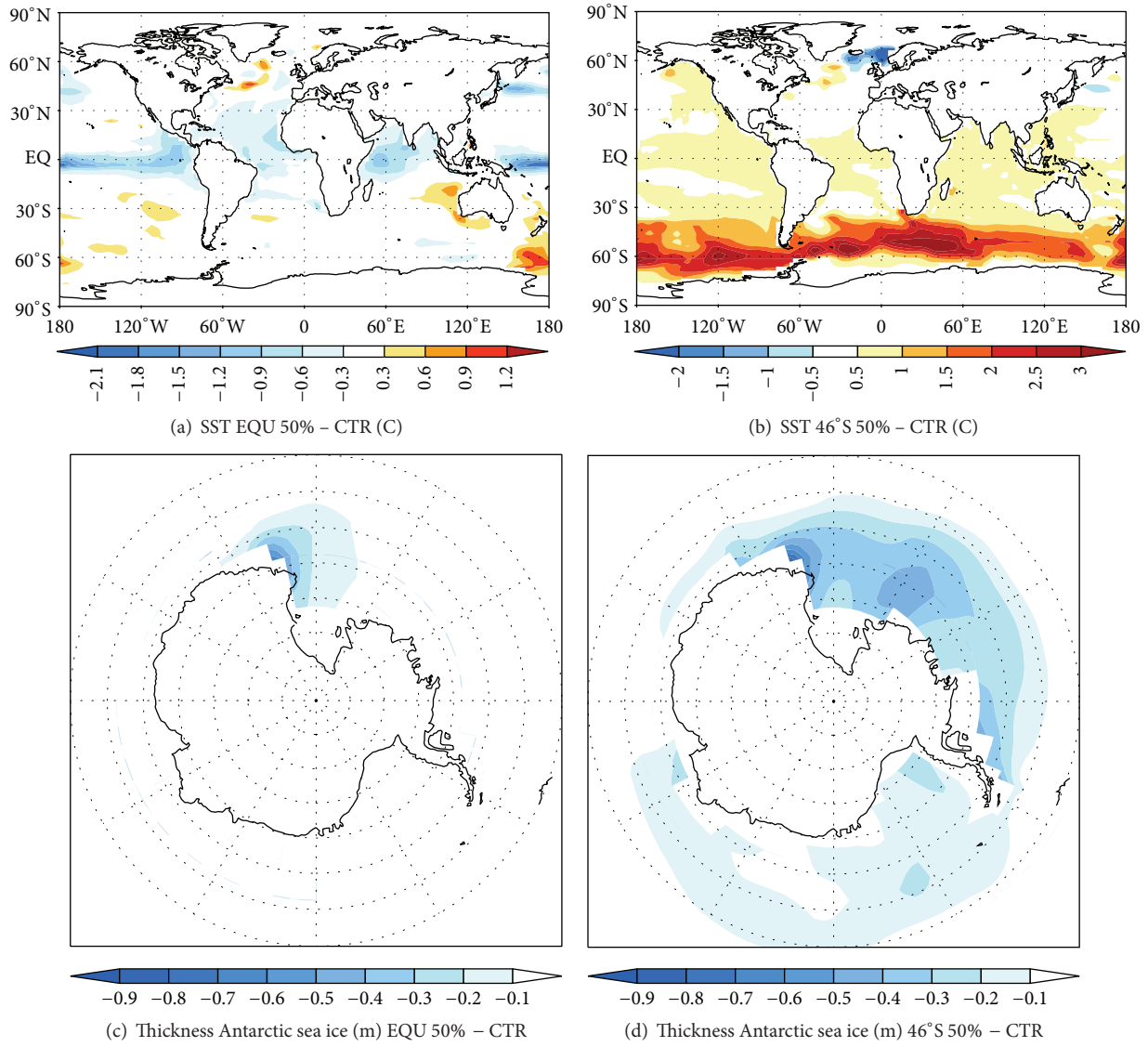

Figure 2: (a) SST anomalies (°C) for EQU 50% – CTR, (b) SST anomalies (°C) for 46°S 50% – CTR, (c) Thickness Antarctic sea ice anomaly (m) for EQU 50% – CTR, and (d) thickness Antarctic sea ice anomalies (m) for 46°S 50% – CTR.

influenced by increased upwelling negative anomalies are dominant in the western Pacific.

The simulations with the SPEEDO model show changes in SST patterns, favoring changes in the Antarctic sea ice thickness. Figures 2(c) and 2(d) show anomalies in the Antarctic sea ice thickness for both simulations (EQU 50% and 46°S 50%) as compared to CTR. The increased wind stress in the equatorial region causes little modifications on sea ice (Figure 2(c)). However, a reduction in thickness is observed from 50 to 60 cm for Ross Sea region. The link between the equatorial SST and the sea ice variability was previously noted by Yuan [41] and Kwok and Comiso [42].

The intensification of the wind stress in the region of 46°S (Figure 2(d)) shows an overall reduction in the sea ice thickness around Antarctica with substantial anomalies (values of up to 60–70 cm) occurring in the Ross, Bellingshausen, and Amundsen Seas. In a twofold manner, the melting of sea ice allows higher SST values leading to further reduction of sea ice thickness. This dynamic feedback is associated with larger absorption of solar radiation and reinforces the initial heating [43].

3.1.2. Global Thermohaline Circulation. Changes on the oceanic characteristics in the extratropical and polar regions can affect the rate of deep water formation in both hemispheres [44, 45]. Figure 3 shows the average flow of the Atlantic Meridional Overturning Circulation (MOC) at 30°W longitude for the last 20 years of the CTR simulation by EQU 50% and 46°S 50% experiments. It is demonstrated that in the CTR experiment (Figure 3(a)) there is a southward transport of water with values between 8 and 12 Sv, associated with the NADW between 30°N and 50°N in a depth ranging

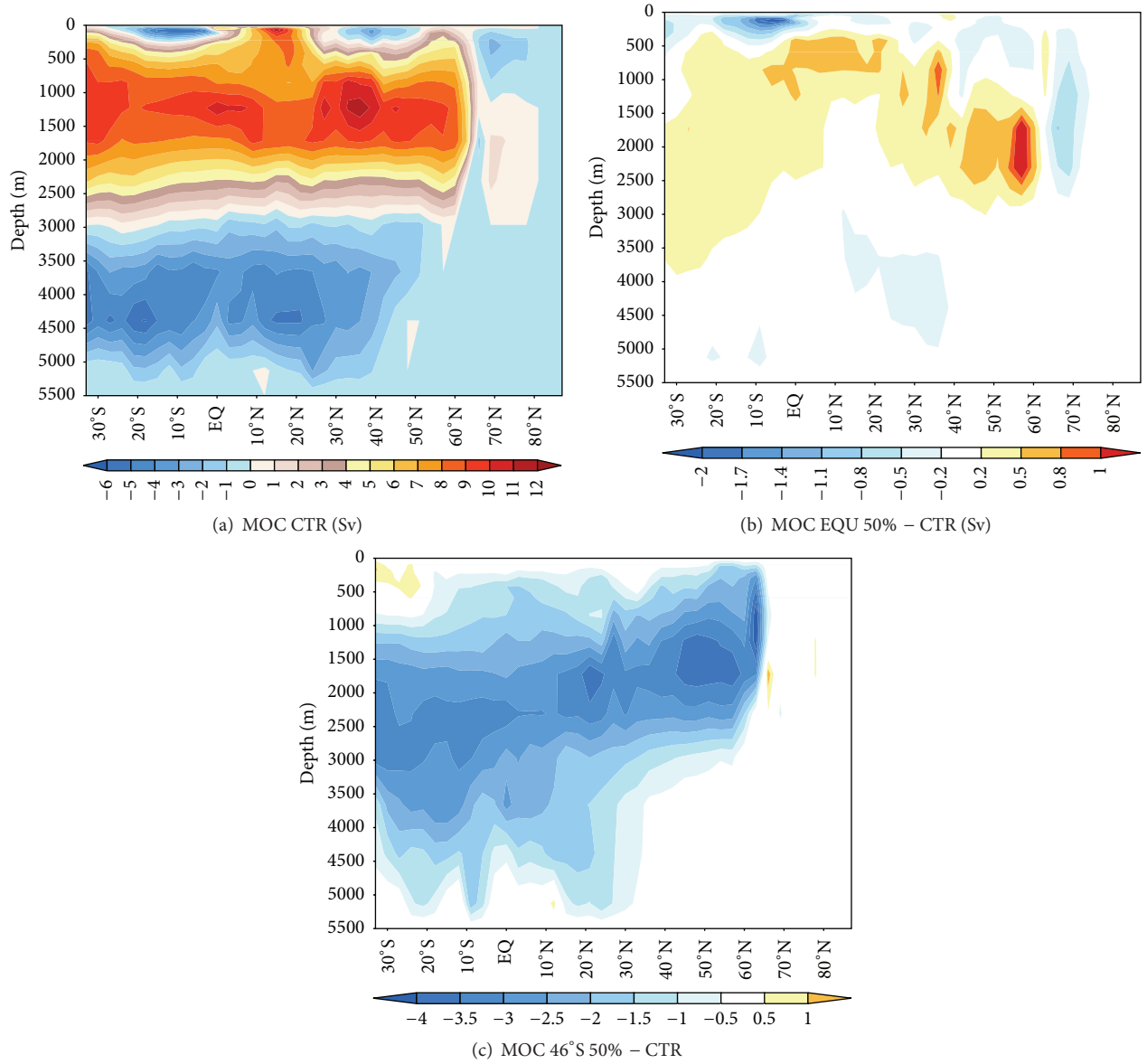

(a) MOC CTR (Sv)

(b) MOC EQU 50% − CTR (Sv)

(c) MOC 46°S 50% − CTR

Figure 3: Annual thermohaline global circulation average for Atlantic Ocean (Sv). (a) CTR simulation, (b) difference of experiments for EQU 50% – CTR, and (c) difference of experiments for 46°S 50% – CTR.

from 500 to 2000 meters. The underneath northward flow is related to the formation of the Antarctic Bottom Water (AABW) with values reaching −6 Sv.

It is important to remark that SPEEDO underestimates the NADW, when compared to results found by Talley et al. [46] using observations and Gent [47] based on the NCAR model results. Both show NADW maxima by about 20 Sv. Cunningham et al. [48] found 18.7 Sv from observations. However, SPEEDO maximum stream function in the North Atlantic can reach values up to 16 Sv. The global (Atlantic + Pacific + Indian) AABW strength of 12 Sv is in close agreement with observation and other modeling results [49].

The THC anomalies between CTR and EQU 50% experiment (Figure 3(b)) demonstrate that the intensification of winds stress in the equatorial region leads to slight intensification of the NADW (1 Sv) between 40°N and 60°N. However, no changes are observed with respect to AABW. Timmermann and Goosse [6] highlight that this intensification on trade winds strengthens the subtropical gyres in the Atlantic and consequently increases the transport of saline waters to extratropical latitudes. However, in EQU 50% simulation, an increase of the 1 Sv in NADW does not cause significant changes in THC.

By intensifying the wind in the region of 46°S, changes in THC are observed. In this new climate scenario, there is a weakening of NADW by about 4 Sv distributed throughout the Atlantic from 500 meters to 2000 meters of depth (Figure 3(c)), which is accompanied by a strengthening in

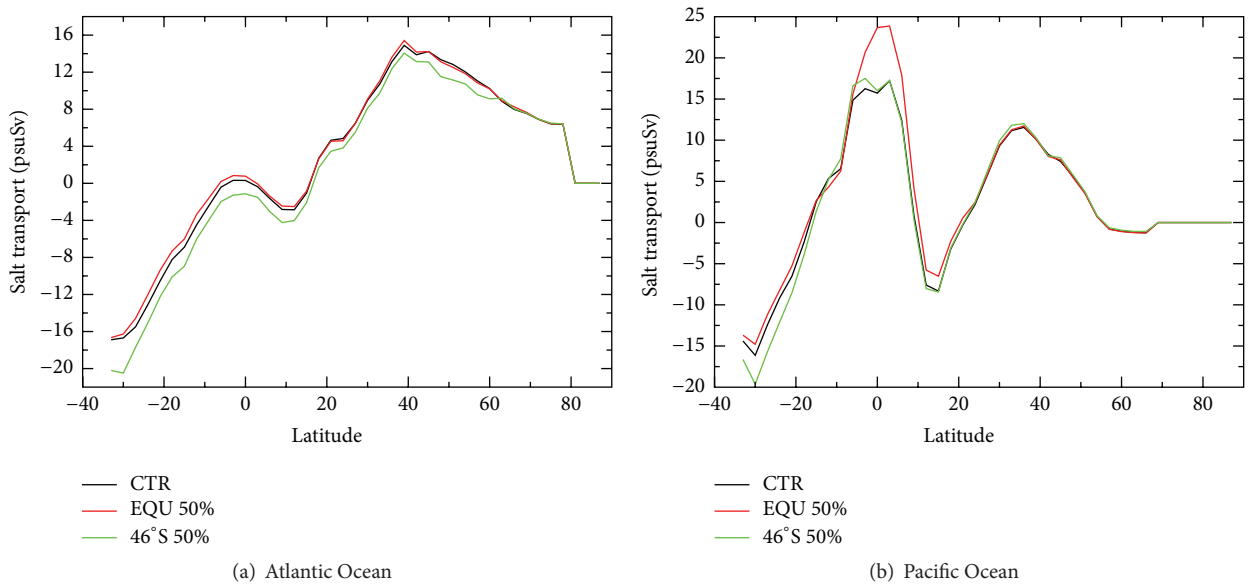

Figure 4: Annual salt transport zonally averaged (Sv). (a) Atlantic Ocean and (b) Pacific Ocean. Black line: CTR simulation; red line: EQU 50% simulation; and green line: 46°S 50% simulation.

the AABW in the 46°S 50% experiment. As will be discussed later, changes in the NADW further lead to changes in the oceanic heat transport which plays a substantial role in driving SST and sea ice. Through the magnitude anomalies of ocean current between 46°S 50% and CTR experiments (not shown), there is an occurrence of negative anomalies in the North Atlantic, which shows the weakening of the Gulf Stream in this situation. This condition contributes to lower transport salt and heat and as a result weakens the APAN. This explains the negative SST anomalies in the North Atlantic (Figure 2(b)). This is in agreement with results proposed by Menviel et al. [8], which found an increase in the transport of AABW associated with more vigorous winds near the surface and an increase of SST in the same region. Numerical simulations suggest that a change in Agulhas leakage, due to changes of the winds in extratropical regions of the Southern Hemisphere, can impact the thermohaline properties of the Atlantic Ocean and hence stratification and deep convection formation, which are directly linked to MOC [50]. Justino et al. [34] by analysing the climate response to reduced Antarctic ice sheet height argued that reducing the sea ice thickness and allowing for enhanced heat loss from the ocean surface to the atmosphere increase the water density underneath the mixing layer favoring convection. The second effect that can lead to a strengthening of the AABW formation rate is associated with the heat-salt distribution of subsurface water.

However, different results are found by Delworth and Zeng [40] that report an intensification of THC in deeper layers, by considering stronger and southward wind stress in the Southern Ocean. Hirabara et al. [51] also highlighted that an intensification of the wind stress in the Southern Ocean promotes an intensification of NADW as a response to the baroclinic wave propagation to the North Atlantic.

3.1.3. Salt Transport. Despite the importance of salinity to deep water formation, the influence of wind stress changes on the salt transport in both equatorial and extratropical belts has been partially overlooked. In the following the salt transport changes in the Atlantic and Pacific oceans due to modification in the wind stress are discussed. Figures 4(a) and 4(b) show the zonal average salt transport in the Atlantic and Pacific oceans for CTR, EQU 50%, and 46°S 50% experiments.

The salt transport analyses in Atlantic Ocean show that the simulations forced with increased wind stress do not differ substantially from the CTR outside the region of the applied forcing. The maximum values occur in the region of 40° latitude in both hemispheres, linked to the contribution of the Gulf Stream in transporting saline waters into the North Atlantic and in the SH associated with the Brazil current in the South Atlantic.

It should be noted that the transport of salt is intensified (reduced) in the South (North) Atlantic in the 46°S 50% experiment. Figure 4(a) shows an intensification of 4 Sv at 35°S. The opposite occurs in the North Atlantic, where the salt transport decreases between 40°N and 60°N. This anomalous pattern contributes to an increase in the salinity in the South Atlantic but favors a reduction in the North Atlantic, insofar the salt contribution is concerned. This salt transport feature is in agreement with the response of the THC to wind stress changes previously discussed.

Figure 4(b) shows the zonal averaged salt transport in the Pacific Ocean. In the EQU 50% simulation, it is clear that the increase of the wind stress in the equatorial region generates an additional northward salt transport by up to 10 Sv, as compared to the CTR simulation. This remarkable change occurs in the equatorial belt, whereas changes in

the northern hemisphere are smaller. The intensification of the wind stress in 46°S 50% experiment indicates that changes in the Pacific Ocean salt transport are more intense in the SH, where there is an increase in the transport of about 5 Sv between 30°S and 40°S. This anomalous pattern of the salt transport is in agreement with increase in salinity in the vicinity of the Antarctic ocean (not shown).

3.2. Atmospheric Changes

3.2.1. Baroclinic Instability. Large-scale temperature and atmospheric circulation changes have potential to modify the statistics of transient and steady waves. This is predominantly generated by baroclinic instabilities from the background flow, which has been attributed to enhanced meridional/zonal thermal contrast [52]. It is worth mentioning that the baroclinic and barotropic instability mechanisms are responsible for the formation and maintenance of waves and eddies that act regulating the heat and momentum balance in oceanic frontal regions. One good example is the tropical instability waves that occur in the equatorial regions of the Pacific [53] and the Atlantic [54].

The Eady growth rate (σ_{b1}) is computed in the mid-troposphere at 500 hPa level, in order to investigate changes to atmospheric baroclinicity induced by the wind stress anomalies. This is a simplified measure of atmospheric baroclinicity that can be employed to quantify the potential for instabilities and cyclone growth [52, 55]. The Eady growth rate estimates baroclinic instability from the vertical wind shear and the static stability of the atmosphere. It is defined as

$$\sigma_{b1} = 0.31 \frac{f}{N} \left(\frac{\partial V}{\partial Z} \right), \tag{2}$$

where f is the Coriolis parameter, N the Brunt-Väisälä frequency, Z the upward vertical coordinate, and V the horizontal wind speed.

Figures 5(a) and 5(b) show the averaged σ_{b1} for the CTR simulation, for December-January-February (DJF) and June-July-August (JJA), respectively. Negative values for the SH and positive values for the Northern Hemisphere are related with the Coriolis parameter. The σ_{b1} is more intense on each hemisphere during the winter period due to higher thermal contrasts over the mid-latitudes and consequently associated with stronger wind shear [56]. The maximum values are observed between Asia and North Pacific and over the SH mid-latitudes and Antarctica (Figures 5(a) and 5(b)).

Figures 5(c) and 5(d) show the baroclinic activity anomalies as a result of the wind stress intensification over the equatorial region during DJF and JJA. Note that during DJF (Figure 5(c)), there are no significant anomalies in the Southern Hemisphere. This result is reasonable since no remarkable changes are simulated in the atmospheric circulation. On the other hand, stronger baroclinic activity is predicted to occur in the NH mid-latitudes and extratropical regions. These anomalies of σ_{b1} in the Northern Hemisphere follow changes in the vertical wind profile (not shown). During JJA, small changes in σ_{b1} occur on both hemispheres (Figure 5(d)).

By changing wind stress in the Southern Ocean (Figures 5(e) and 5(f)), a reduction σ_{b1} (positive anomalies) is demonstrated, mainly between 45°S and 60°S. Differences of σ_{b1} between the 46°S 50% and CTR experiment during JJA are shown in Figure 5(f); we obtain a reduction of the baroclinic activity in the SH around 60°S. One can argue that the reduction of the thermal gradient between the tropics and the extratropical region and the consequent weakening of the westerlies can promote the reduction of the baroclinic activity in this climate scenario.

3.2.2. Storminess. Changes in the atmosphere baroclinic structure are closely linked to transient eddy anomalies, more commonly known as storm. Storm track is often defined by the regions where there is a maximum variance of geopotential height in the upper and mid-troposphere, arising from disturbances with periods less than one week approximately [52, 57]. According to Wu et al. [58], the storms act as regulators of the precipitation. These transient eddies are also responsible for large part of the poleward heat transport reducing the meridional thermal gradient between the tropics and the polar regions [59]. Therefore, changes in the position and magnitude of the storms can influence heat, moisture, and momentum transports in the atmosphere [60].

In this study, storms are estimated in terms of the eddy heat flux ($\overline{v'T'}$) at 700 hPa and eddy momentum flux ($\overline{u'v'}$) at 200 hPa, both for DJF and JJA periods. It is important to highlight that $\overline{v'T'}$ represents the exchange between basic state potential energy and potential energy available for the disturbances. The $\overline{u'v'}$ characterizes the exchange between kinetic energy of the disturbances and kinetic energy of the basic state [61].

The activity of the eddy heat flux ($\overline{v'T'}$) at 700 hPa is shown in Figure 6 as well as its anomalies between the wind stress experiments and the CTR simulation for DJF and JJA. It should be noted that the ($\overline{v'T'}$) is intensified over mid-latitudes and high latitudes during the winter season in each hemisphere (Figures 6(a) and 6(b)), with maximum values ranging from −25 to 35 Km s^{-1}. According to Trenberth [56], the intensified jet in winter favors the eastward advection of the transient waves. The SPEEDO model underestimates the magnitude of the storms when compared to finer resolution models. The continuous pattern of the storms in the Southern Ocean when compared with the Northern Hemisphere is remarkable.

Figures 6(c) and 6(d) show $\overline{v'T'}$ anomalies during DJF and JJA between the EQU 50% and the CTR experiments. Stronger storm activity is noted over the northern part of Eurasia and Nordic Seas but reduced activity over the northern Pacific in DJF (Figure 6(c)). No changes are predicted to occur during JJA. Seager et al. [62] argued that changes in the tropical Pacific due to ENSO events generate anomalous pattern of storm tracks. Indeed, the EQU 50% experiment resembles a permanent La Niña-like event and therefore may alter the wave propagation paths.

Eddy heat flux ($\overline{v'T'}$) anomalies between the 46°S 50% experiment and the CTR simulation during the summer and winter in both hemispheres are shown in Figures 6(e) and 6(f). During DJF (Figure 6(e)) there are no significant

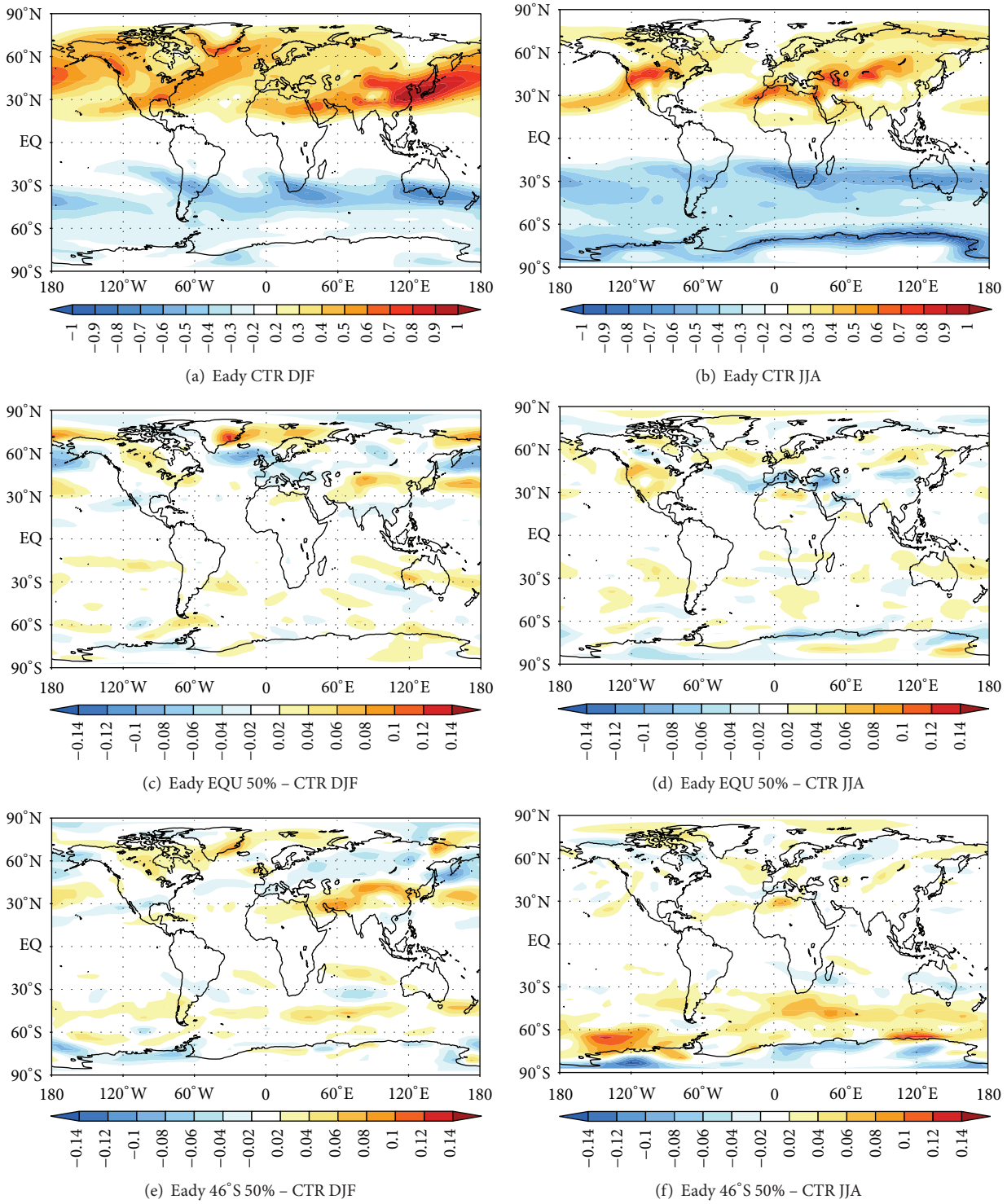

(a) Eady CTR DJF

(b) Eady CTR JJA

(c) Eady EQU 50% – CTR DJF

(d) Eady EQU 50% – CTR JJA

(e) Eady 46°S 50% – CTR DJF

(f) Eady 46°S 50% – CTR JJA

FIGURE 5: Baroclinic instability (σ_{b1}): (a) CTR simulation in DJF, (b) CTR simulation in JJA, (c) EQU 50% – CTR in DJF, (d) EQU 50% – CTR in JJA, (e) 46°S 50% – CTR in DJF, and (f) 46°S 50% – CTR in JJA. Units are in day^{-1}.

anomalies. However, a weakening of the eddy momentum flux is observed in the North Pacific and Atlantic Ocean. Changes on the pattern of storms during SH winter (Figure 6(f)) depict positive values (weaker $\overline{v'T'}$) throughout the Southern Ocean, primarily due to the overall warming over extratropical latitudes as predicted to occur under stronger wind stress forcing.

The second storm quantity evaluated is the upper troposphere eddy momentum flux ($\overline{u'v'}$) at 200 hPa (Figure 7). $\overline{u'v'}$ is directly associated with the westerly flow on both

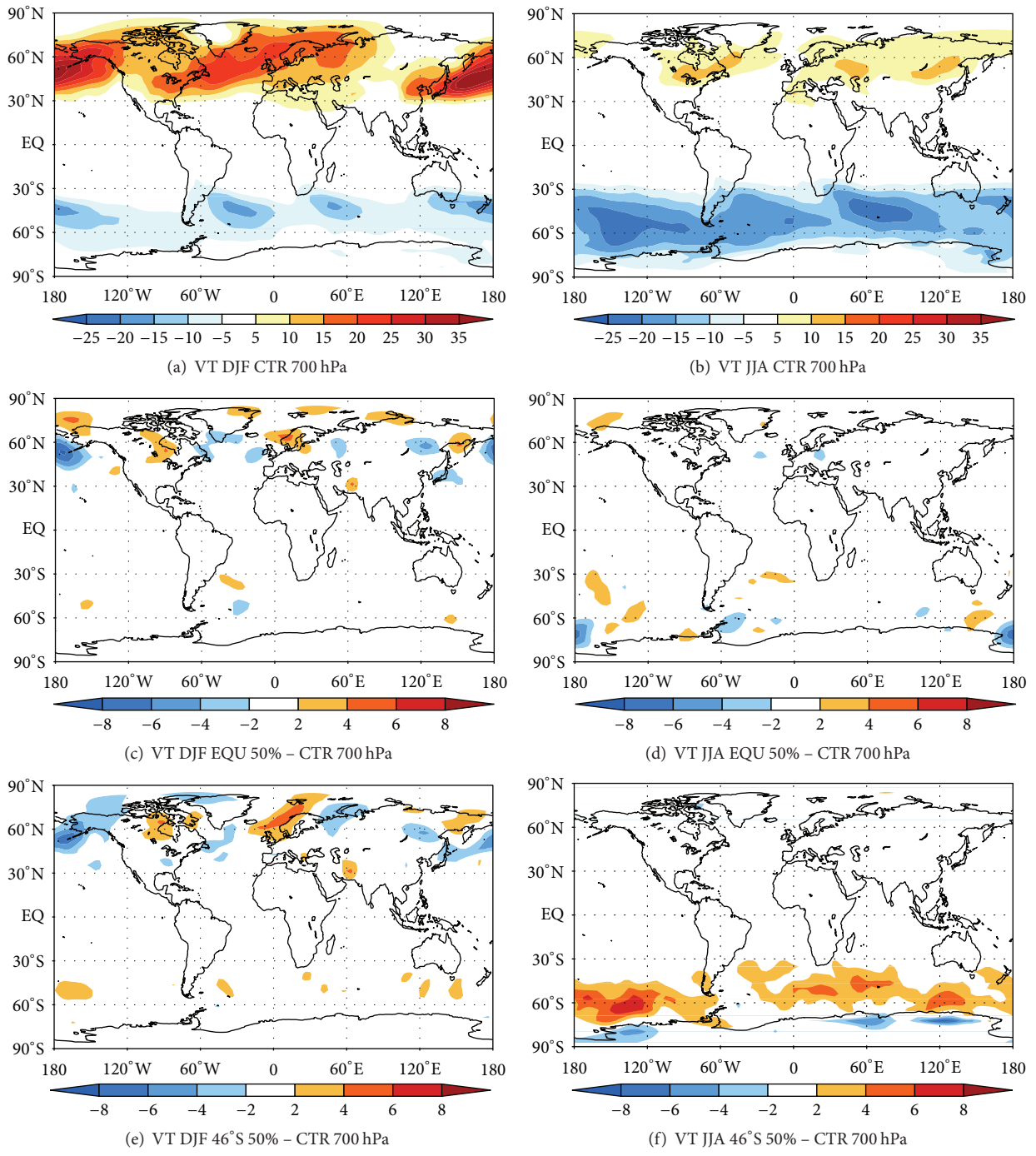

FIGURE 6: Eddy heat flux ($\overline{v'T'}$). (a) CTR simulation in DJF, (b) CTR simulation in JJA, (c) EQU 50% − CTR in DJF, (d) EQU 50% − CTR in JJA, (e) 46°S 50% − CTR in DJF, and (f) 46°S 50% − CTR in JJA. Units are in km s^{-1}.

hemispheres and is more intense during DJF (JJA) in the Northern (Southern) Hemisphere (Figures 7(a) and 7(b)). In the Southern Hemisphere $\overline{u'v'}$ is predominantly confined between 30° and 45°S in both seasons. In the NH $\overline{u'v'}$ spatial distribution and magnitude exhibit stronger seasonal cycle as compared to the SH.

Figures 7(c) and 7(d) show anomalies of $\overline{u'v'}$ between CTR and EQU 50% experiments for DJF and JJA. As shown for $\overline{v'T'}$, the intensification of wind stress in the equatorial region does not contribute significantly to changes in the storm tracks pattern but enhanced activity is noted over Hudson Bay and Japan Sea/Eastern Asia in DJF (Figure 7(c)).

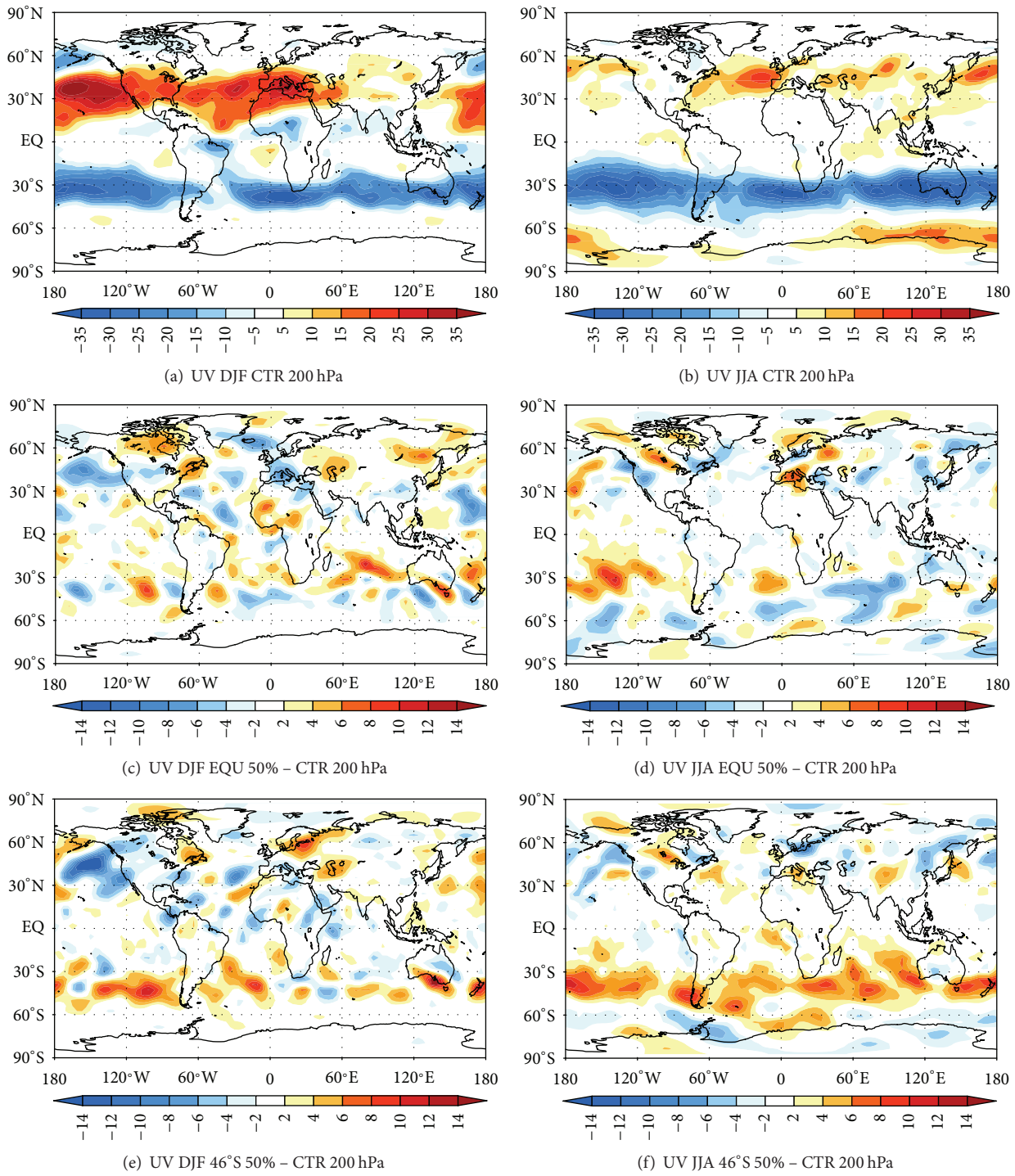

(a) UV DJF CTR 200 hPa

(b) UV JJA CTR 200 hPa

(c) UV DJF EQU 50% – CTR 200 hPa

(d) UV JJA EQU 50% – CTR 200 hPa

(e) UV DJF 46°S 50% – CTR 200 hPa

(f) UV JJA 46°S 50% – CTR 200 hPa

Figure 7: Eddy momentum flux ($\overline{u'v'}$). (a) CTR simulation in DJF, (b) CTR simulation in JJA, (c) EQU 50% – CTR in DJF, (d) EQU 50% – CTR in JJA, (e) 46°S 50% – CTR in DJF, and (f) 46°S 50% – CTR in JJA. Units are in $m^2\ s^{-2}$.

During JJA in the Southern Hemisphere (Figure 7(d)), positive values are observed at Pacific Ocean in the region of 30°S. This indicates a storm weakening for EQU 50% simulation as compared to the unperturbed CTR conditions.

For 46°S 50% simulation (Figures 7(e) and 7(f)), the largest differences occur over Southern Hemisphere mid-latitudes during JJA (Figure 7(f)), $\overline{u'v'}$ is weakened by $12\ m^2/s^2$ between 30°S and 45°S. It is important to point out that the wind stress intensification in mid-latitudes also leads

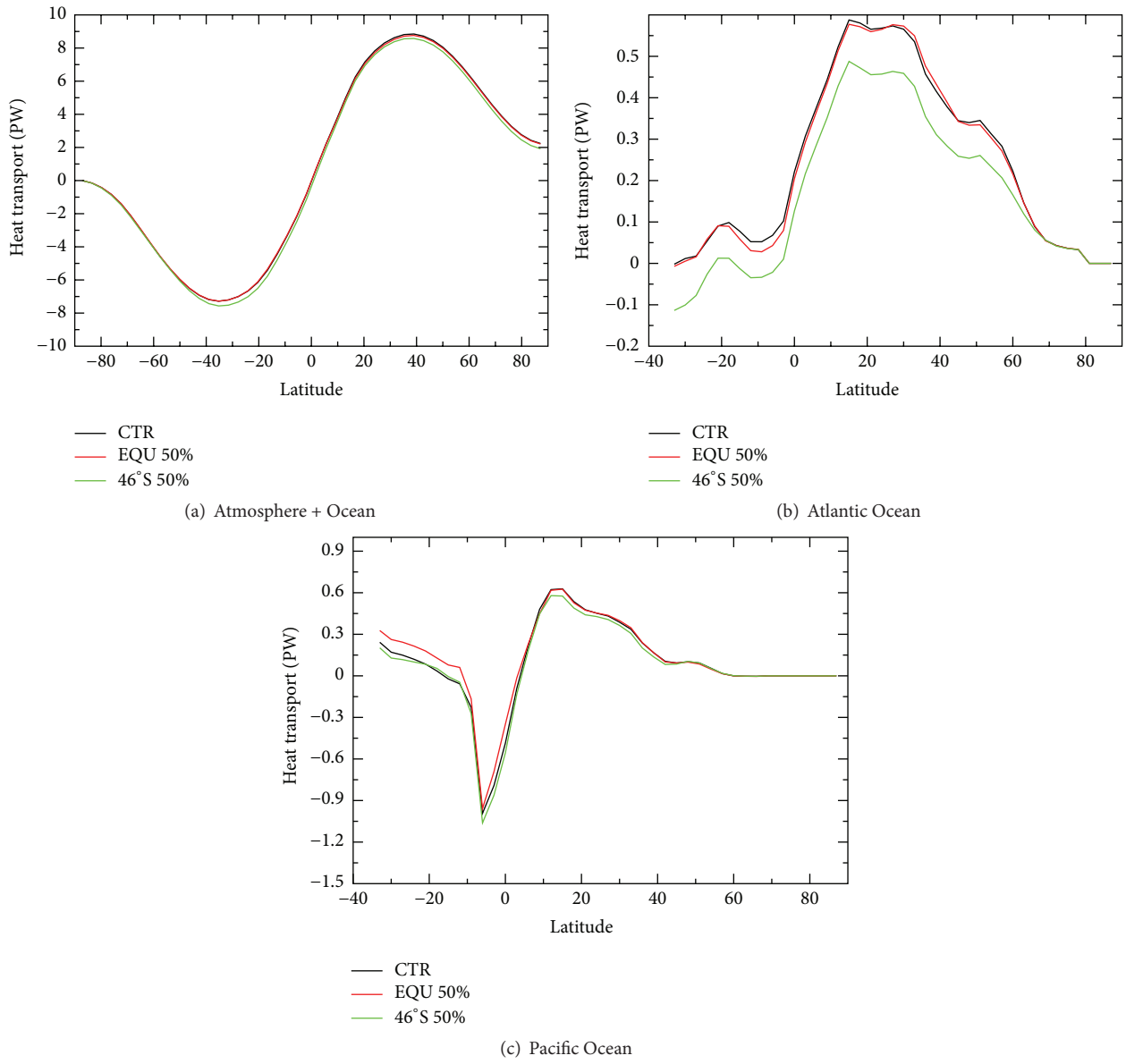

Figure 8: Heat transport zonally averaged (PW). (a) Total heat transport, (b) heat transport in Atlantic Ocean, and (c) heat transport in Pacific Ocean. Black line: CTR simulation, red line: EQU 50% simulation, and green line: 46°S 50% simulation.

to weaker baroclinic instability and $\overline{v'T'}$ at 700 hPa. This was not anticipated because enhanced zonal wind stress at mid-latitudes should be associated with stronger meridional thermal gradient and atmospheric baroclinicity.

Recently, Justino et al. [34] performed numerical simulations with SPEEDO coupled model using a modified Antarctic topography. Their results indicate that modifications of the Antarctic ice sheet height induce a weakening of the meridional thermal gradient and $\overline{v'T'}$ and $\overline{u'v'}$.

3.2.3. Total Poleward Heat Transport. As discussed earlier, the intensification of wind stress in the equatorial region and the Southern Ocean favors the occurrence of anomalies in atmospheric and oceanic circulations. These changes may be associated with anomalies in the atmospheric and oceanic poleward heat transport. The total poleward heat transport of the ocean-atmosphere system in each latitudinal band is computed from the difference between net shortwave radiation and outgoing long-wave radiative flux at the top of the atmosphere [63–65]. It can be expressed as

$$H(\phi)_{\text{total}} = H_{\text{ATM}} + H_{\text{OCE}} = 2a^2\pi \int \left(S_{\text{TOA}}(\phi)' - L_{\text{TOA}}(\phi)'\right) \cdot \cos\phi' \cdot d\phi', \quad (3)$$

where H_{total}, H_{ATM}, and H_{OCE} are the total, atmospheric, and oceanic heat transports, a is the radius of the Earth, ϕ is the latitude, S_{TOA} is the zonal averaged net shortwave radiation, and L_{TOA} is the zonal averaged outgoing long-wave radiation. Both fluxes are computed at the top of the atmosphere.

Table 1: Heat transport at 30°S for the numerical experiments. Units are PW.

Experiments	Total heat transport	Global ocean	Atlantic	Indi./Pac.	Atmosphere
CTR	−7.21	−0.86	0.01	−1.04/0.17	−6.35
EQU 50%	−7.21	−0.92	0.01	−1.19/0.26	−6.29
46°S 50%	−7.52	−1.12	−0.10	−1.14/0.12	−6.40

Table 2: Heat transport in 30°N for the numerical experiments. Units are PW.

Experiments	Total heat transport	Global Ocean	Atlantic	Pac.	Atmosphere
CTR	8.63	0.96	0.57	0.39	7.67
EQU 50%	8.53	0.97	0.57	0.40	7.56
46°S 50%	8.38	0.82	0.46	0.36	7.56

Figure 8 shows zonal averaged total heat transport (Ocean + Atmosphere) and the oceanic contribution for the Atlantic and Pacific regions for the CTR, EQU 50%, and 46°S 50% simulations. The sum of the heat transport from the ocean and the atmosphere (Figure 8(a)) shows a similar pattern between the CTR and the simulations forced with the intensification of wind stress. The maximum values of total heat transport occur between the latitudes of 30° and 40° at both hemispheres. Negative (positive) values indicate heat transport towards the South (North) Pole. The SPEEDO model simulates the total heat transport with values close to those seen in Trenberth and Caron [65] and Wu et al. [58]; however, the model overestimates this transport up to 1 PW at 30° latitude in both hemispheres. It should be noted that the values proposed in the literature are based on reanalysis and uncertainties are still present.

By analyzing the total heat transport between CTR and EQU 50% experiments small differences are observed (Table 1). In the Northern Hemisphere, the total heat transport is weakened in the EQU 50% simulation in 0.1 PW in 30°N (Table 2). However, the total heat transport is substantially modified when the wind stress is intensified in the Southern Ocean. This situation is evident in Figure 8(a), where there is a heat transport intensification in the Southern Hemisphere and a weakening in the Northern Hemisphere. By analyzing Tables 1 and 2, it should be noted that the total heat transport increases by up to 0.31 PW at 30°S, while in the Northern Hemisphere a weakening of 0.25 PW occurs. This southward heat transport increase in the Southern Hemisphere can favor an increase of SST and air temperature over the extratropical region. Thus, the ocean transport of heat changes direction, favoring the formation process of the interhemispheric seesaw. According to Broecker [66], a reduction in deep water formation rates of the South Atlantic or the North Atlantic should occur, so that this phenomenon occurs. Machado et al. [45] also show this process due to a weakening in the MOC. Although the ocean heat transport contributes only 10% of the total, the results show that a small enhancement associated with a change of direction contributes significantly to changes in atmospheric and ocean circulations in this climate scenario.

When considering only the contribution of heat transport of the Atlantic and Pacific oceanic regions (Figures 8(b) and 8(c)), it is clear that the maximum values occur in the equatorial region. From Tables 1 and 2 one may note that the oceanic heat transport contributes to about 15% of the total transport. The impact of the intensification of the wind stress in the oceanic heat transport is remarkable on 46°S 50% experiment. Specifically, changes on heat transport occur significantly in the Atlantic Ocean (Figure 8(b)). The oceanic heat transport is intensified in the South Atlantic and the opposite occurs in the North Atlantic. It should be noted that this is in close agreement with the changes in the THC. It is well known that the THC contributes significantly with the transport of heat from the Southern to the Northern Hemisphere as well as from the Atlantic to Indian-Pacific basins [67, 68].

4. Conclusions and Final Remarks

Based on simulations conducted by the climate model SPEEDO, the atmospheric and oceanic response to wind stress anomalies applied in the equatorial (EQU 50%) and extratropical region (46°S 50%) was evaluated. It has been demonstrated that the forcing applied on the equatorial and the Southern Ocean regions leads to different responses of the climate system. When the wind stress is enhanced over the equatorial region (EQU 50% experiment) an intensification of the Ekman transport and consequent acceleration of the oceanic subtropical cells was verified leading to an equatorial cooling due to the increased upwelling and evaporation.

By increasing the wind stress over the Southern Ocean (46°S 50%), there is a local warming of the sea surface up to 3°C and a reduction in the Antarctic sea ice thickness. On the other hand the North Atlantic is cooled down. This anomalous negative SST pattern is associated with the North Atlantic Deep Water formation rate decreasing and an increasing in the Antarctic Bottom Water. Thus, the total heat transport (Ocean + Atmosphere) is affected and it is most related by changes in the oceanic heat transport, in the Atlantic Ocean.

This increased wind stress in the Southern Ocean induces the positive temperature anomalies found around the Antarctic region. This fact is an evident consequence from the intensification of heat fluxes exchanges between the ocean and the atmosphere. The warming in the Southern Hemisphere

favors the slowdown of the jet stream due to the meridional weakening of the thermal gradient. As a result, the baroclinic instability and storm are reduced.

It is noteworthy that, with the simulations, it can be concluded that upwelling is the mechanism responsible for changes in oceanic and atmospheric circulations when the wind stress is intensified in the equatorial region. However, changes in ocean patterns for extratropical regions, due to the wind stress intensification, need further investigation, since the answer is not yet clear when you compare our results with other works. Thus, it is important to conduct similar modeling experiments based on climate models with higher degree of complexity, involving more vertical atmospheric layers and recent developments in cloud parameterization.

Conflict of Interests

The authors declare that there is no conflict of interests regarding the publication of this paper.

Acknowledgment

This research has been supported by the CNPq Project Proposals 407681/2013-2 and 305586/2012-2.

References

[1] G. T. Walker and E. W. Bliss, "World Weather V," *Memoirs of the Royal Meteorological Society*, vol. 4, no. 36, pp. 53–84, 1932.

[2] J. Bjerknes, "Atlantic air-sea interaction," *Advances in Geophysics*, vol. 10, pp. 1–82, 1964.

[3] K. Wyrtki, "Teleconnections in the equatorial Pacific Ocean," *Science*, vol. 180, no. 4081, pp. 66–68, 1973.

[4] F. Justino, *The influence of glacial boundary conditions on the climate system during the last glacial maximum [Ph.D. thesis]*, Leibniz Institute of Marine Sciences, Kiel, Germany, 2004.

[5] L. P. Pezzi, J. Vialard, K. J. Richards, C. Menkes, and D. Anderson, "Influence of ocean-atmosphere coupling on the properties of Tropical Instability Waves," *Geophysical Research Letters*, vol. 31, no. 16, Article ID L16306, 2004.

[6] A. Timmermann and H. Goosse, "Is the wind stress forcing essential for the meridional overturning circulation?" *Geophysical Research Letters*, vol. 31, no. 4, Article ID L04303, 2004.

[7] X.-Y. Yang, R. X. Huang, and D. X. Wang, "Decadal changes of wind stress over the Southern Ocean associated with Antarctic ozone depletion," *Journal of Climate*, vol. 20, no. 14, pp. 3395–3410, 2007.

[8] L. Menviel, A. Timmermann, A. Mouchet, and O. Timm, "Climate and marine carbon cycle response to changes in the strength of the Southern Hemispheric westerlies," *Paleoceanography*, vol. 23, no. 4, Article ID PA4201, 2008.

[9] O. A. Saenko, "On the climatic impact of wind stress," *Journal of Physical Oceanography*, vol. 39, no. 1, pp. 89–106, 2009.

[10] H. Ma, L. X. Wu, and C. Li, "The role of southern high latitude wind stress in global climate," *Advances in Atmospheric Sciences*, vol. 27, no. 2, pp. 371–381, 2010.

[11] N. P. Gillett and D. W. J. Thompson, "Simulation of recent Southern Hemisphere climate change," *Science*, vol. 302, no. 5643, pp. 273–275, 2003.

[12] J. C. Fyfe and O. A. Saenko, "Simulated changes in the extratropical Southern Hemisphere winds and currents," *Geophysical Research Letters*, vol. 33, no. 6, Article ID L06701, 2006.

[13] J. C. Fyfe, O. A. Saenko, K. Zickfeld, M. Eby, and A. J. Weaver, "The role of poleward-intensifying winds on Southern Ocean warming," *Journal of Climate*, vol. 20, no. 21, pp. 5391–5400, 2007.

[14] N. C. Swart and J. C. Fyfe, "Observed and simulated changes in the Southern Hemisphere surface westerly wind-stress," *Geophysical Research Letters*, vol. 39, no. 16, Article ID L16711, 2012.

[15] J. McCreary and P. Lu, "Interaction between the subtropical and the equatorial ocean circulations: the subtropical cell," *Journal of Physical Oceanography*, vol. 24, pp. 466–497, 1994.

[16] Z. Liu and S. Philander, "How different wind stress pattern affect the tropical-subtropical circulations of the upper ocean," *Journal of Physical Oceanography*, vol. 25, pp. 449–462, 1995.

[17] A. B. G. Bush and S. G. H. Philander, "The climate of the Last Glacial Maximum: results from a coupled atmosphere-ocean general circulation model," *Journal of Geophysical Research: Atmospheres*, vol. 104, no. 20, Article ID 1999JD900447, pp. 24509–24525, 1999.

[18] S.-I. An, A. Timmermann, L. Bejarano et al., "ENSO dynamics during the Last Glacial Maximum," *Paleoceanography*, vol. 19, pp. 1–11, 2004.

[19] A. Timmermann, F. Justino, F.-F. Jin, U. Krebs, and H. Goosse, "Surface temperature control in the North and tropical Pacific during the last glacial maximum," *Climate Dynamics*, vol. 23, no. 3-4, pp. 353–370, 2004.

[20] M. H. England, S. McGregor, P. Spence et al., "Recent intensification of wind-driven circulation in the Pacific and the ongoing warming hiatus. The world ocean thermohaline circulation," *Nature Climate Change*, vol. 4, pp. 222–227, 2014.

[21] D. G. MacMynowski and E. Tziperman, "Two-way feedback interaction between the thermohaline and wind-driven circulations," *Journal of Physical Oceanography*, vol. 36, no. 5, pp. 914–929, 2006.

[22] J. R. Toggweiler, "Shifting westerlies," *Science*, vol. 323, no. 5920, pp. 1434–1435, 2009.

[23] J. R. Toggweiler and J. Russell, "Ocean circulation in a warming climate," *Nature*, vol. 451, no. 7176, pp. 286–288, 2008.

[24] R. F. Anderson, S. Ali, L. I. Bradtmiller et al., "Wind-driven upwelling in the southern ocean and the deglacial rise in atmospheric CO_2," *Science*, vol. 323, no. 5920, pp. 1443–1448, 2009.

[25] J. Marshall and K. Speer, "Closure of the meridional overturning circulation through Southern Ocean upwelling," *Nature Geoscience*, vol. 5, no. 3, pp. 171–180, 2012.

[26] T. A. Shaw and O. Pauluis, "Tropical and subtropical meridional latent heat transports by disturbances to the zonal mean and their role in the general circulation," *Journal of the Atmospheric Sciences*, vol. 69, no. 6, pp. 1872–1889, 2012.

[27] J. P. Machado, F. Justino, and L. P. Pezzi, "Efeitos do aumento da tensão de cisalhamento do vento no clima do Hemisfério Sul obtido do modelo acoplado SPEEDO," *Revista Brasileira de Meteorologia*, vol. 29, no. 4, pp. 597–612, 2014.

[28] C. A. Severijns and W. Hazeleger, "The efficient global primitive equation climate model SPEEDO V2.0," *Geoscientific Model Development*, vol. 3, no. 1, pp. 105–122, 2010.

[29] W. Bourke, "A multilevel spectral model. I. Formulation and hemispheric integrations," *Monthly Weather Review*, vol. 102, no. 10, pp. 687–701, 1974.

[30] I. Held and M. Suarez, "A two-level primitive equation atmosphere model designed for climate sensitivity experiments," *Journal of the Atmospheric Sciences*, vol. 35, pp. 206–229, 1978.

[31] F. Molteni, "Atmospheric simulations using a GCM with simplified physical parametrizations. I: model climatology and variability in multi-decadal experiments," *Climate Dynamics*, vol. 20, no. 2-3, pp. 175–191, 2003.

[32] F. Kucharski, F. Molteni, and A. Bracco, "Decadal interactions between the western tropical Pacific and the North Atlantic Oscillation," *Climate Dynamics*, vol. 26, no. 1, pp. 79–91, 2006.

[33] A. Bracco, F. Kucharski, R. Kallummal, and F. Molteni, "Internal variability, external forcing and climate trends in multi-decadal AGCM ensembles," *Climate Dynamics*, vol. 23, no. 6, pp. 659–678, 2004.

[34] F. Justino, J. Marengo, F. Kucharski, F. Stordal, J. Machado, and M. Rodrigues, "Influence of Antarctic ice sheet lowering on the Southern Hemisphere climate: modeling experiments mimicking the mid-Miocene," *Climate Dynamics*, vol. 42, no. 3-4, pp. 843–858, 2014.

[35] H. Goosse and T. Fichefet, "Importance of ice-ocean interactions for the global ocean circulation: a model study," *Journal of Geophysical Research*, vol. 104, no. 10, Article ID 1999JC90215, pp. 23337–23355, 1999.

[36] G. L. Mellor and T. Yamada, "Development of a turbulence closure model for geophysical fluid problems," *Reviews of Geophysics and Space Physics*, vol. 20, no. 4, pp. 851–875, 1982.

[37] P. Gent and J. McWilliams, "Isopycnal mixing in ocean general circulation model," *Journal of Physical Oceanography*, vol. 20, pp. 150–155, 1990.

[38] L. F. Klinger, Q. J. Li, A. B. Guenther, J. P. Greenberg, B. Baker, and J. H. Bai, "Assessment of volatile organic compound emissions from ecosystems of China," *Journal of Geophysical Research: Atmospheres D*, vol. 107, no. 21, pp. ACH 16-1–ACH 16-21, 2002.

[39] J. Yang, "The seasonal variability of the Arctic Ocean Ekman transport and its role in the mixed layer heat and salt fluxes," *Journal of Climate*, vol. 19, no. 20, pp. 5366–5387, 2006.

[40] T. L. Delworth and F. R. Zeng, "Simulated impact of altered Southern Hemisphere winds on the Atlantic Meridional Overturning Circulation," *Geophysical Research Letters*, vol. 35, no. 20, Article ID L20708, 2008.

[41] X. Yuan, "ENSO-related impacts on Antarctic sea ice: a synthesis of phenomenon and mechanisms," *Antarctic Science*, vol. 16, no. 4, pp. 415–425, 2004.

[42] R. Kwok and J. C. Comiso, "Southern Ocean climate and sea ice anomalies associated with the Southern Oscillation," *Journal of Climate*, vol. 15, no. 5, pp. 487–501, 2002.

[43] F. Justino, F. Hastenreiter, and A. Grimm, "Impacto do dióxido de carbono atmosférico no gelo marinho Antártico," *Oecologia Brasiliensis*, vol. 11, no. 1, pp. 69–77, 2007.

[44] R. J. Stouffer, J. Yin, J. M. Gregory et al., "Investigating the causes of the response of the thermohaline circulation to past and future climate changes," *Journal of Climate*, vol. 19, no. 8, pp. 1365–1387, 2006.

[45] J. P. Machado, F. Justino, and L. P. Pezzi, "Changes in the global heat transport and eddy-mean flow interaction associated with weaker thermohaline circulation," *International Journal of Climatology*, vol. 32, no. 15, pp. 2255–2270, 2012.

[46] L. D. Talley, J. L. Reid, and P. E. Robbins, "Data-based meridional overturning streamfunctions for the global ocean," *Journal of Climate*, vol. 16, no. 19, pp. 3213–3226, 2003.

[47] P. R. Gent, "Will the North Atlantic Ocean thermohaline circulation weaken during the 21st century?" *Geophysical Research Letters*, vol. 28, no. 6, pp. 1023–1026, 2001.

[48] S. A. Cunningham, T. Kanzow, D. Rayner et al., "Temporal variability of the Atlantic meridional overturning circulation at 26.5°N," *Science*, vol. 317, no. 5840, pp. 935–938, 2007.

[49] A. H. Orsi, G. C. Johnson, and J. L. Bullister, "Circulation, mixing, and production of antarctic bottom water," *Progress in Oceanography*, vol. 43, no. 1, pp. 55–109, 1999.

[50] R. J. Haarsma, E. J. D. Campos, S. Drijfhout, W. Hazeleger, and C. Severijns, "Impacts of interruption of the Agulhas leakage on the tropical Atlantic in coupled ocean-atmosphere simulations," *Climate Dynamics*, vol. 36, no. 5-6, pp. 989–1003, 2011.

[51] M. Hirabara, H. Ishizaki, and I. Ishikawa, "Effects of the westerly wind stress over the Southern Ocean on the meridional overturning," *Journal of Physical Oceanography*, vol. 37, no. 8, pp. 2114–2132, 2007.

[52] B. J. Hoskins and P. J. Valdes, "On the existence of storm tracks," *Journal of the Atmospheric Sciences*, vol. 47, no. 15, pp. 1854–1864, 1990.

[53] L. P. Pezzi and K. J. Richards, "Effects of lateral mixing on the mean state and eddy activity of an equatorial ocean," *Journal of Geophysical Research C*, vol. 108, no. 12, article 3371, 2003.

[54] A. C. V. Caltabiano, I. S. Robinson, and L. P. Pezzi, "Multi-year satellite observations of instability waves in the Tropical Atlantic Ocean," *Ocean Science*, vol. 1, no. 2, pp. 97–112, 2005.

[55] C. J. Paciorek, J. S. Risbey, V. Ventura, and R. D. Rosen, "Multiple indices of Northern Hemisphere cyclone activity, winters 1949–99," *Journal of Climate*, vol. 15, no. 13, pp. 1573–1590, 2002.

[56] K. E. Trenberth, "Storm tracks in the Southern Hemisphere," *Journal of the Atmospheric Sciences*, vol. 48, pp. 2151–2178, 1991.

[57] F. Justino, A. Timmermann, U. Merkel, and E. P. Souza, "Synoptic reorganization of atmospheric flow during the last glacial maximum," *Journal of Climate*, vol. 18, no. 15, pp. 2826–2846, 2005.

[58] Y. Wu, M. Ting, R. Seager, H.-P. Huang, and M. A. Cane, "Changes in storm tracks and energy transports in a warmer climate simulated by the GFDL CM2.1 model," *Climate Dynamics*, vol. 37, no. 1, pp. 53–72, 2011.

[59] K. E. Trenberth, "The role of eddies in maintaining the westerlies in the Southern Hemisphere winter," *Journal of the Atmospheric Sciences*, vol. 44, no. 11, pp. 1498–1508, 1987.

[60] J. H. Yin, "A consistent poleward shift of the storm tracks in simulations of 21st century climate," *Geophysical Research Letters*, vol. 32, no. 18, Article ID L18701, pp. 1–4, 2005.

[61] A. M. C. Carmo, *Os Storm Tracks no Hemisfério Sul. Tese (Doutorado em Meteorologia)*, Instituto Nacional de Pesquisas Espaciais, São Paulo, Brazil, 2004.

[62] R. Seager, N. H. Naik, M. F. Ting, M. A. Cane, N. Harnik, and Y. Kushnir, "Adjustment of the atmospheric circulation to tropical pacific sst anomalies: variability of transient eddy propagation in the pacific-north america sector," *Quarterly Journal of the Royal Meteorological Society*, vol. 136, no. 647, pp. 277–296, 2010.

[63] J. R. Miller and G. L. Russell, "Ocean heat transport during the last glacial maximum," *Paleoceanography*, vol. 4, no. 2, pp. 141–155, 1989.

[64] J. Peixoto and A. Oort, *Physics of Climate*, Springer, 1992.

[65] K. E. Trenberth and J. M. Caron, "Estimates of meridional atmosphere and ocean heat transports," *Journal of Climate*, vol. 14, no. 16, pp. 3433–3443, 2001.

[66] W. S. Broecker, "Paleocean circulation during the last deglaciation. A bipolar seesaw?" *Paleoceanography*, vol. 13, no. 2, pp. 119–121, 1998.

[67] K. Döös, J. Nilsson, J. Nycander, L. Brodeau, and M. Ballarotta, "The world ocean thermohaline circulation," *Journal of Physical Oceanography*, vol. 42, no. 9, pp. 1445–1460, 2012.

[68] M. Vellinga and R. A. Wood, "Global climatic impacts of a collapse of the atlantic thermohaline circulation," *Climatic Change*, vol. 54, no. 3, pp. 251–267, 2002.